https://doi.org/10.5194/egusphere-2026-889
Preprint. Discussion started: 16 March 2026

On some factors controlling fission-track etch rates in apatite

Raymond Jonckheere[1*], Florian Trilsch[1], Jie Liu[2], Pengfei Zhai[2], Thorsten Nagel[1]

[1]Endogene Geologie, Technische Universität Bergakademie Freiberg, Deutschland

[2]Institute of Modern Physics, Chinese Academy of Sciences, Lanzhou, Gansu 730000, China

Abstract

Fission tracks in apatite must be etched to be counted and measured with an optical microscope. Track etching is described with the aid of two velocities: the track etch rate v_T and the apatite etch rate v_R. On their values depend the efficiencies of track counts, the selection of confined tracks for measurement, and the shapes of etched tracks; v_R is an indicator of the apatite composition and annealing kinetics. In spite of this, direct measurements of v_T and v_R have long been wanting. This work provides numerical data and investigates factors controlling v_T and v_R. The results indicate that v_T is constant over most of the ion- and fission-fragment ranges in apatite (constant core). We observed that, when using a step-etch protocol, the etchant advances at a high, but finite, rate along tracks etched in a preceding step. Thus, step-etching broadens the effective-etch-time distribution, and the summed etch time overestimates the aggregate effect of the procedure. Neither annealing of induced tracks nor ageing of fossil tracks has a measurable effect on v_T. Since the v_T-value along a particular track section does not depend on its radius or on the work expended to create it, it can be considered characteristic of an apatite instead of a track. This could account for the different v_T of the Duluth and Durango apatites. The identical distributions of the host-confined-track intersections, ***c***-axis angles, and track-etch rates across all experiments suggests that confined-track selection is little dependent on the track densities or lengths, but dominated by a condition that is unaffected by annealing. In contrast to v_T, v_R exhibits clear variation related to radiation damage from natural background radiation in the case of fossil tracks and from neutron irradiation in case of induced. Greater v_R shorten the access times to confined tracks, increasing their effective etch times. This implies a need for caution when using Dpar to assess the annealing kinetics.

Keywords

Apatite, fission track, etching, track etch rate, apatite etch rate

*corresponding author: raymond.jonckheere@geo.tu-freiberg.de

https://doi.org/10.5194/egusphere-2026-889
Preprint. Discussion started: 16 March 2026

1. Introduction

The fission-track method is a useful tool for dating rocks and retracing their low-temperature thermal histories, based on counting and measuring the damage trails from uranium fission in minerals. Apatite is the most studied mineral, and the focus of this investigation. Fission tracks in apatite shorten and fade through a range of temperatures relevant to geological processes such as basin subsidence and uplift, erosional and tectonic unroofing, thrust tectonics, and hydrocarbon maturation. Apatite grains separated from a rock are mounted in resin, polished and etched for examination with a microscope. Etching creates straight channels along the damage trails left by the fission fragments. In contrast to unetched tracks, which have nanometre diametres, etched tracks have micrometre diameters, suitable for counting and measuring. From the beginning, track etching has been described in terms of two velocities: the etch rate, v_T, of the damaged lattice along the track and the bulk etch rate, v_B, of the undamaged apatite in all other directions (Fleischer and Price, 1964; Hurford, 2019). Their values determine the etching and counting efficiencies of different crystal faces (Gleadow, 1981; Tagami and O'Sullivan, 2005), and the roundedness of the confined track tips (Ketcham and Tamer, 2021). These factors determine which grains are suitable for counting and dating and which tracks are suitable for measurement and Tt-modelling.

Little is known for certain about the factors that affect the apatite and track etch rates. It is known that v_B is anisotropic (Gleadow, 1981), and also depends on the apatite composition (Burtner et al., 1994; Carlson et al., 1999). We know less about v_T, which is assumed constant (Laslett et al., 1984) or related to the track radius or damage density (Ketcham and Tamer, 2021; Li et al., 2023). Earlier, following established concepts of crystal dissolution (Gross, 1918; Heimann, 1975; 1982), we redefined the apatite etch rate as the rate of displacement of a lattice plane (v_R; Jonckheere et al., 2019; 2022) instead of that of each point on a surface (v_B). We investigated how v_R varies with composition (Trilsch et al. 2023; Fu et al., 2024) and with orientation, noting steep minima parallel and perpendicular to the ***c***-axis (Aslanian et al., 2021). Here we investigate factors affecting v_R and v_T. Section 2 focusses on the variation of v_T along tracks, section 3 on the effect of annealing, and section 4 on that of ageing on v_R and v_T. The discussion is based on the cumulative frequencies of the measured quantities. Additional scatter plots and histograms are presented in the supplements.

2. Variation of v_T

We mounted a prism section of Durango apatite in resin, ground, and polished it with 6-µm, 3-µm, and 1-µm diamond suspensions and a 0.04-µm silica suspension to expose an even internal surface. We covered the mount with 180-µm Al degrader and 12-µm PET film, and irradiated it perpendicular to the ***c***-axis and at 45° dip angle with 25.0 MeV.amu^{-1} ^{86}Kr-ions at the HIRFL in Lanzhou, operated by the Institute of Modern Physics of the Chinese Academy of Sciences (Figure 1). We etched the mount in 5.5 M HNO_3 at 21 °C for 20 s + 10 s + 10 s to reveal the tracks (Figure 2). The sample had a sealed natural crack extending from the surface to tens of microns below it. Although no etchant could penetrate along it, the crack nevertheless constituted a break in the apatite lattice. The intersections of the Kr-tracks with the crack are therefore convex, like their intersections with the surface, causing etch figures bounded by the fastest etching faces to develop (Aslanian et al., 2021; Jonckheere et al., 2022). This produces uniform etch pits at the apatite surface, one side of which, with length Dpar, is parallel to the ***c***-axis (Burtner et al., 1994). The same process takes place on either side of the crack, giving rise to diamond-shaped etch figures, which decrease in size at increasing distances along the track from its surface intersection (Figure 2a).

https://doi.org/10.5194/egusphere-2026-889
Preprint. Discussion started: 16 March 2026

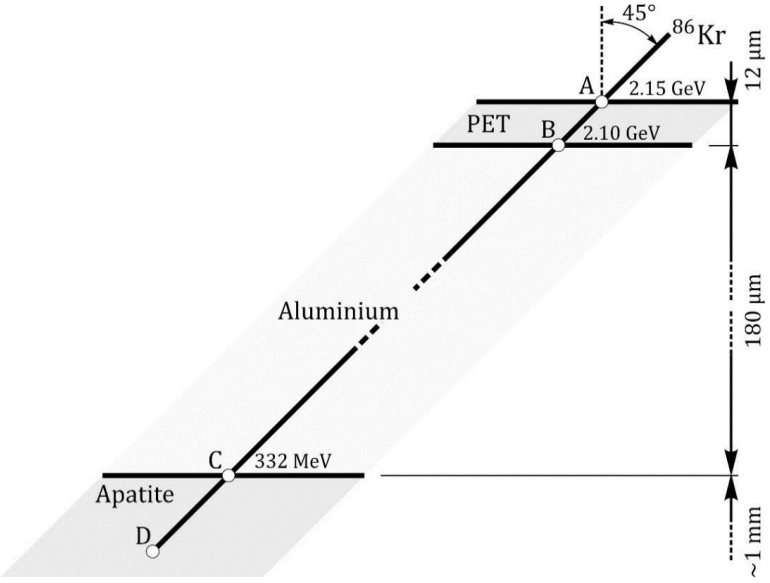

Figure 1. Kr irradiation: a prism section of an unannealed single Durango apatite is covered with a 180 µm Al degrader and a 12 µm PET film, and irradiated perpendicular to the apatite ***c***-axis and at 45° dip angle with 25.0 MeV/amu ^{86}Kr. The samples were etched in 5.5 M HNO_3 at 21 °C for 20 s + 10 s + 10 s to reveal the tracks.

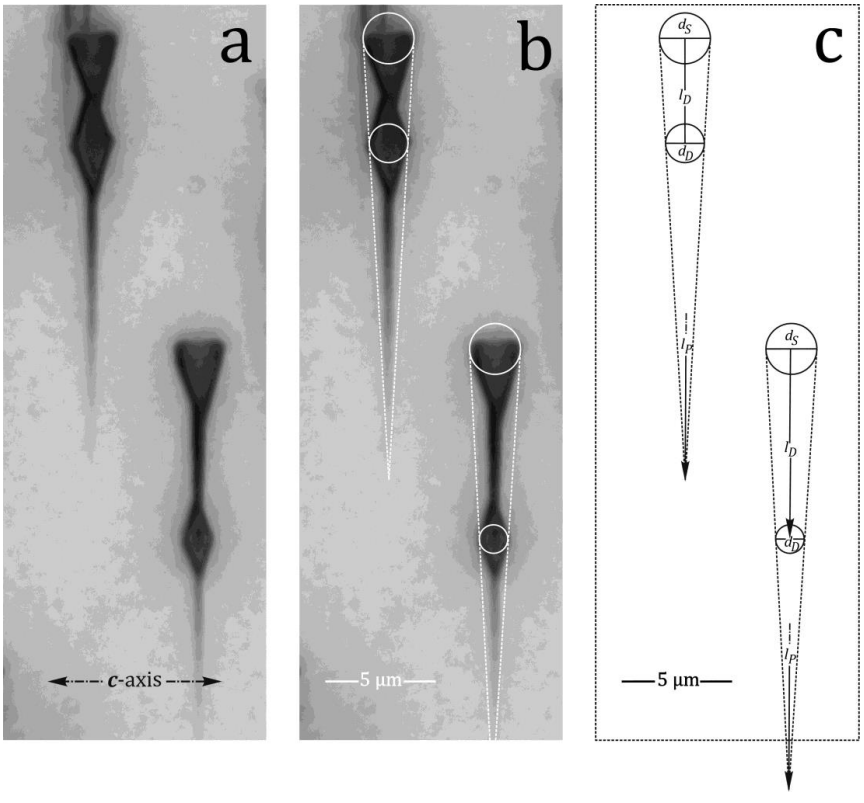

Figure 2. Kr tracks etched in 5.5 M HNO_3 at 21 °C for 20 s (**a**, **b**), the measurements are indicated in (**c**).

https://doi.org/10.5194/egusphere-2026-889
Preprint. Discussion started: 16 March 2026

From their respective sizes (d_S, d_D) and the immersion times (t_I) we calculated the effective etch times $t_E = (d_D / d_S)\, t_I$, and access times, $t_A = t_I - t_E$, of the diamond shapes, i.e., the time required for the etchant to advance along the track from the surface to the crack. Figure 2b illustrates the measurements of d_S, d_D, and $l = l_D / \cos(¼\pi)$ and the total projected length $l_M = l_P / \cos(¼\pi)$. Table 1 reports the measurements for the 20-, 30-, and 40-s cumulative immersion times. Figure 3a plots d_D against l; Figure 3b shows histograms of the calculated lengths l_M. The solid lines in Figure 3a are geometric mean regression lines anchored at the mean values of d_S. These means have negligible error compared to the individual d_D-values, because d_S exhibits almost no variation and was measured for each track and immersion time. Table 1 lists the slopes (s) of the regression lines, along with their d-axis and l-axis intercepts, and the calculated mean track etch rates: $v_T = -d_S / (s\, t_I)$.

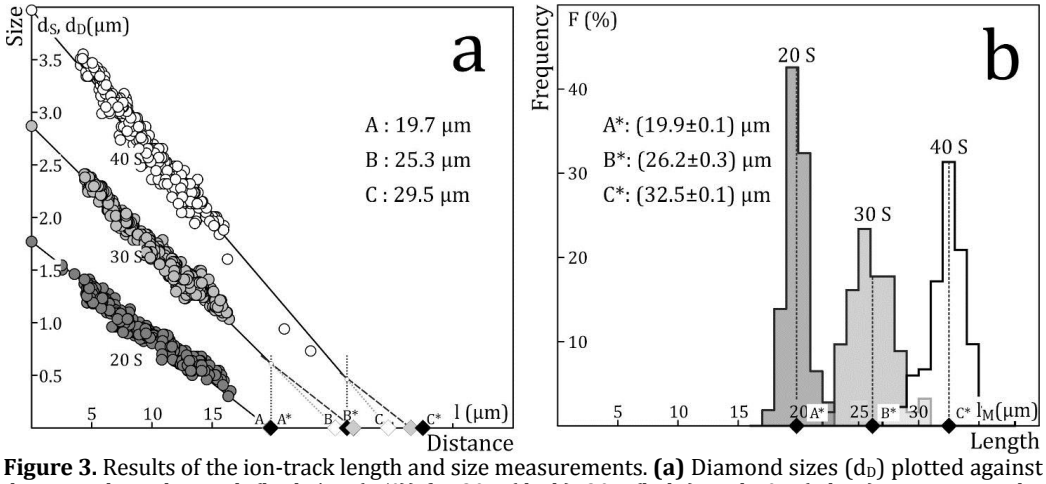

Figure 3. Results of the ion-track length and size measurements. **(a)** Diamond sizes (d_D) plotted against distance along the track ($l = l_D/\cos(45°)$) for 20 s (dark), 30 s (light), and 40 s (white) immersion. The data at l = 0 (d_S) are the average track openings (D_{PAR}). The solid black lines are regression lines anchored at d_S. The intersections of the regression lines with the l-axis at A (20 s), B (30 s), and C (40 s) are extrapolated total etched lengths at each immersion time (white). The black symbols at A* (20 s), B* (30 s), and C* (40 s) are the corresponding measured values. The dashed lines are extrapolations of the 30 s, and 40 s data at A* and B*, assuming the track rate calculated from the 20 s data applies to the unetched sections beyond A* and B*; **(b)** Histograms of the measured track lengths ($l_M = l_P/\cos(45°)$) after etching for 20 s, (20+ 10) s, and (30 + 10) s in 5.5 M HNO_3 at 21 °C. A*, B*, and C* are the mean lengths plotted in (a) (black symbols).

t_I (s)	n_T	s	v_T	d_I	l_I	l_M	l_E	t_M
20	467	-0.090	59.6	1.77	19.7	19.9	19.8	20.1
30	514	-0.113	276	2.87	25.3	26.2	26.7	32.1
40	363	-0.135	324	3.97	29.5	32.5	31.1	40.8

Table 1. Measurements of Kr-tracks in a Durango apatite prism face etched for 20, 30, and 40 s in 5.5 M HNO_3 at 21 °C. t_I (s): immersion time; n_T: number of tracks; s: slopes of geometrical mean regression lines fitted to d_D vs. l (d_D (µm) and l (µm): size of the diamond-shaped etch figure and its distance from the surface; Figure 2); v_T (µm/min): rate of etchant penetration, calculated from the slopes s; d_I (µm), l_I (µm): d- and l-axis intercepts of the regression lines; l_M (µm), l_E (µm): measured (Figure 3b) and calculated (Figure 3a) mean etched length, assuming a constant track etch rate v_T; t_M (s): immersion times corresponding to the measured mean lengths and calculated etch rates.

https://doi.org/10.5194/egusphere-2026-889
Preprint. Discussion started: 16 March 2026

The v_T-value for the initial 20-s immersion ($v_T \approx 60$ μm.min^{-1}) is the actual track etch rate, whereas the values for 30 s and 40 s measure the fast but finite rate of etchant advance along a pre-etched track. The v_T-estimate is consistent with results for induced fission tracks at high angles to the **c**-axis measured in a prism section of Durango apatite (Jonckheere et al., 2024). The latter results indicate that the sum of the immersion times of a step-etch experiment overestimates the true cumulative etch time. For the Kr-tracks, this amounts to $\gtrsim$4 s for the 10-s step following the initial 20-s immersion; i.e., the time to travel the length (≈20 μm) of pre-etched track section at $v_T \approx 275$ μm.min^{-1} (20 μm /4.6 μm.s^{-1}≈ 4.3 s). The effect is less for shorter fission tracks.

The difference (l_M - l_I) between the measured mean lengths and the l-axis intercepts of the regression line is almost negligible after the initial 20-s etch, but increases with each subsequent step (Table 1; Figure 2). This is because the increased penetration rates during later steps relate to the track sections etched during the previous step, but not to the unetched sections beyond, which etch at the track etch rate v_T. We revised the expected lengths (l_E) based on the measured lengths (l_M) and etch rates (v_T) in Table 1. The agreement between the measured and expected lengths (l_M - l_E) and between the estimated and actual immersion times (t_M - t_I) is good considering the uncertainties. In particular the enhanced rates of penetration weigh on the calculations because they are derived from the small differences between the slopes of the regression lines fitted to the 20-, 30-, and 40-s data. The calculation assumes that v_T is constant over the entire etched track length up to 40 s (constant core; Tamer and Ketcham, 2020). The data in Table 1 are interpreted as supporting this.

Constant v_T agrees with the fact that fission tracks in apatite have straight sides, lacking any curvature due to a variable v_T (Figures 4a and 4b; 'motorboat effect'; Fleischer et al., 1969; 1975; Paretzke et al., 1973; Somogyi and Szalay, 1973; Durrani and Bull, 1987; Nikezić, 2000; Nikezić and Yu, 2003; 2004). This means that v_T is unrelated to (dE/dx) (Tamer and Ketcham, 2020; Ketcham and Tamer, 2021), or to the radius of the latent track (Li et al., 2012; 2014). The most compelling indication is that etched confined tracks show no constriction, interruption or other modification in their midsections, even though the effective fission fragment charges, and thus (dE/dx) and the track radius, are assumed to be near zero at the locus of the fissioned nucleus (Li et al., 2023). We have earlier reported that the average fission track etch rate varies with Dpar (Fu et al., 2024) and with the track orientation, with minima parallel and perpendicular to the ***c***-axis, analogous to the apatite etch rate v_R (Jonckheere et al., 2024). This indicates that v_T is more related to the chemical characteristics of the track detector than to the properties of the fission fragments.

3. Effect of annealing

To investigate the effects of partial annealing on v_T and v_R, we carried out track measurements on four prism sections of Durango apatite that had been pre-annealed, neutron-irradiated and - all bar one - re-annealed to create induced-track populations with mean lengths of ~16 μm (sample 21-2), ~14 μm (21-4), ~12 μm (21-1), and ~10 μm (21-3). The irradiation and annealing conditions are detailed in Ketcham et al. (2015). The track densities measured in transmitted and reflected light are reported in Aslanian et al. (2022). The samples were mounted in resin, polished with 6-μm, 3-μm, and 1-μm diamond and 0.04-μm silica suspensions, and etched for 20 s in 5.5 M HNO_3 at 21 C° (Carlson et al., 1999). The confined tracks were imaged and measured as in Jonckheere (2023). The measurements included the track lengths, orientations, widths, cone-angles, the positions of the host track intersections, and Dpar. From the results we calculated the effective etch times and the apatite and track etch rates, using the equations of Aslanian et al. (2021) and Fu et al. (2024).

https://doi.org/10.5194/egusphere-2026-889
Preprint. Discussion started: 16 March 2026

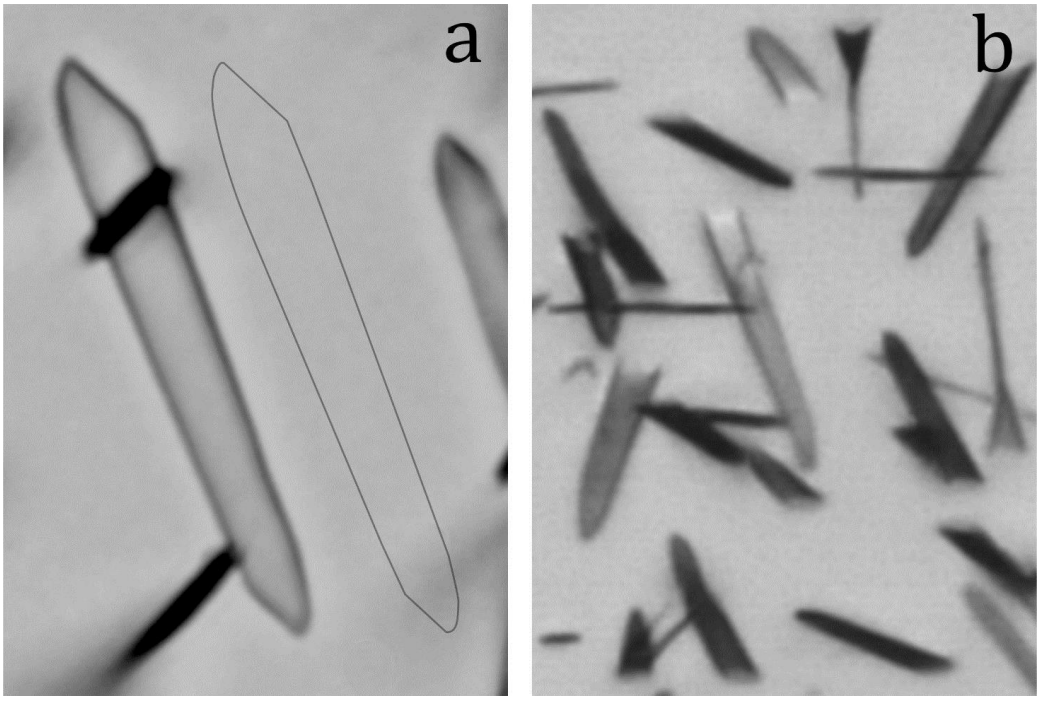

Figure 4. Etched fission tracks in an apatite prism face showing the characteristic straight-sided tapering outline, due to a constant track etch rate v_T: **(a)** horizontal confined track; **(b)** compressed image of surface tracks (etched 20 s in 5.5 M HNO_3 at 21°C).

Figures 5 and 6 show the cumulative distributions of the measured track properties for different annealing stages; Table 2 lists the main statistics. It is surprising to observe that the angular (azimuth) distribution remains unchanged on annealing (Figure 5d). This is similar to the results of Ketcham (2003), except that our data cover mean lengths from 15.9 µm to 10.1 µm, before ***c***-axis projection (Supplement Figure 1d). The intersection-point distribution (from host track to track tip) is also unaffected by annealing (Figure 6a). In each sample, the number of intersections decreases from the centre towards the track tips (Supplement Figure S4) but there is no evidence that, in relative terms, short tracks are differently affected than long tracks. There appears to be no obvious rationale for the invariance of the angular frequencies and of the intersection lengths across the annealing conditions of our samples. These observations are counter to expectation based on length bias and anisotropic annealing (Galbraith et al., 1990; Donelick et al., 1999; Galbraith, 2002; Ketcham, 2003). It has been established that track selection is not just a matter of geometrical biases, but that etching and personal biases must also be taken into consideration. According to Aslanian et al. (2021) and Jonckheere (2023), the selection of a confined track depends on whether it exceeds a threshold width, which is not affected by annealing.

The cumulative v_T-distributions are the same after 10-h annealing at 240 °C (21-4), 288 °C (21-1), and 310 °C (21-3; Figure 5b) as that of unannealed induced tracks (21-2), despite experiencing mean length reductions of ~2, ~4, and ~6 µm. This contradicts the finding that annealing induced tracks at temperatures of 235 °C to 280 °C causes up to a doubling of v_T (Ketcham and Tamer, 2021). Taken together with the fact that v_T exhibits no variation along the tracks (section 2) and is unaffected by lab-annealing, the observations that v_T correlates with Dpar (Fu et al., 2024) and varies with the angle to the apatite ***c***-axis (Jonckheere et al., 2024a) underscore the fact that v_T is more a function of the detector composition than of the damage densities along the fission fragment trajectories.

https://doi.org/10.5194/egusphere-2026-889
Preprint. Discussion started: 16 March 2026

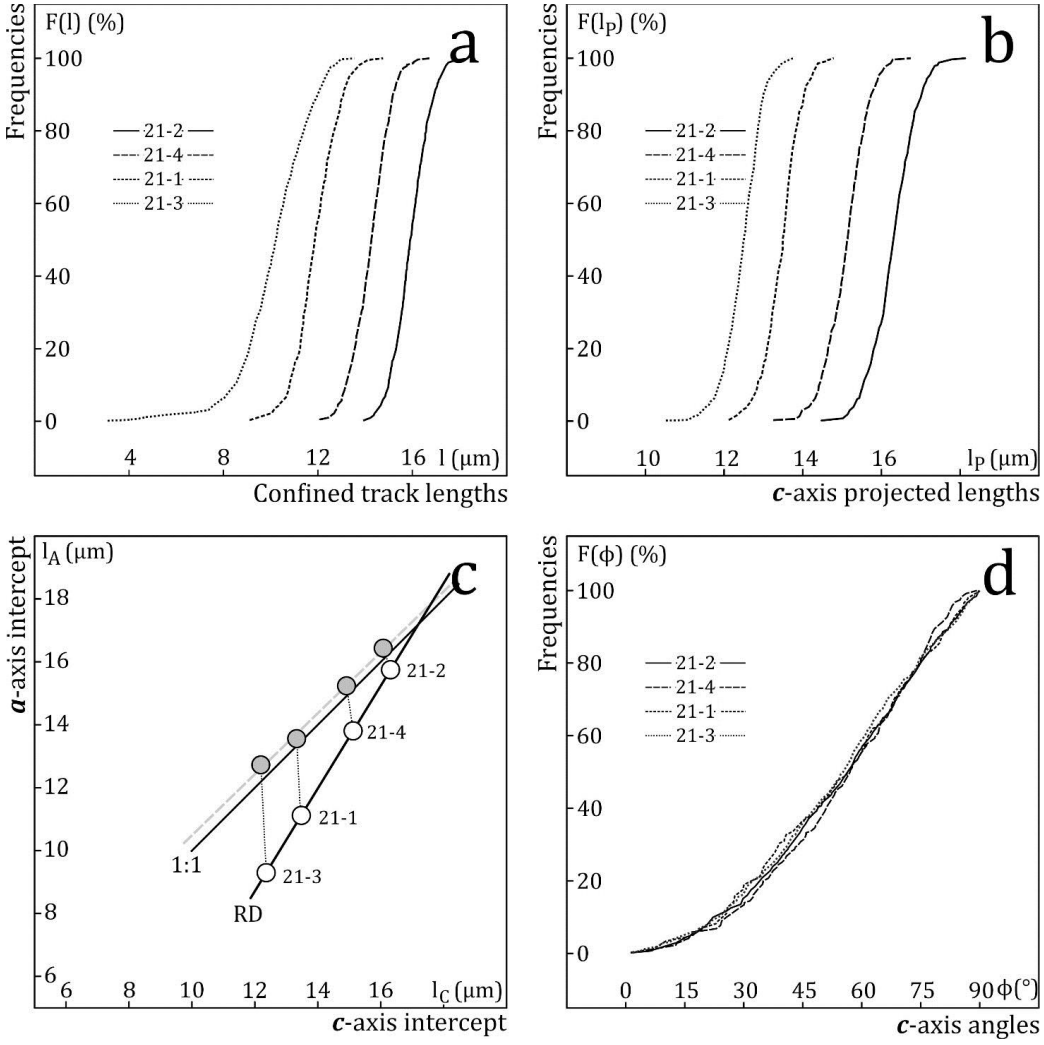

Figure 5. (a) Cumulative frequencies of the lengths of horizontal induced confined tracks in prism faces of four Durango apatites with increasing degrees of annealing, distributed as part of an inter-lab experiment (Ketcham et al., 2015; 21-2: unannealed; 21-4: annealed 10 h at 240 °C; 21-1: annealed 10 h at 288 °C; 21-3: annealed 10 h at 310 °C). **(b)** Cumulative frequencies of the ***c***-axis projected lengths. **(c)** The ***a***-axis vs. ***c***-axis intercepts of ellipses fitted to the length vs. ***c***-axis angle data (white; RD: $l_A = 1.632\ l_C - 10.879$; empirical relationship of Donelick et al., 1999), and of regression lines fitted to the ***c***-axis projected length vs. true ***c***-axis angle (grey; 1:1: isotropic line: $l_A = l_C$); **(d)** cumulative frequencies of the ***c***-axis angles.

https://doi.org/10.5194/egusphere-2026-889
Preprint. Discussion started: 16 March 2026

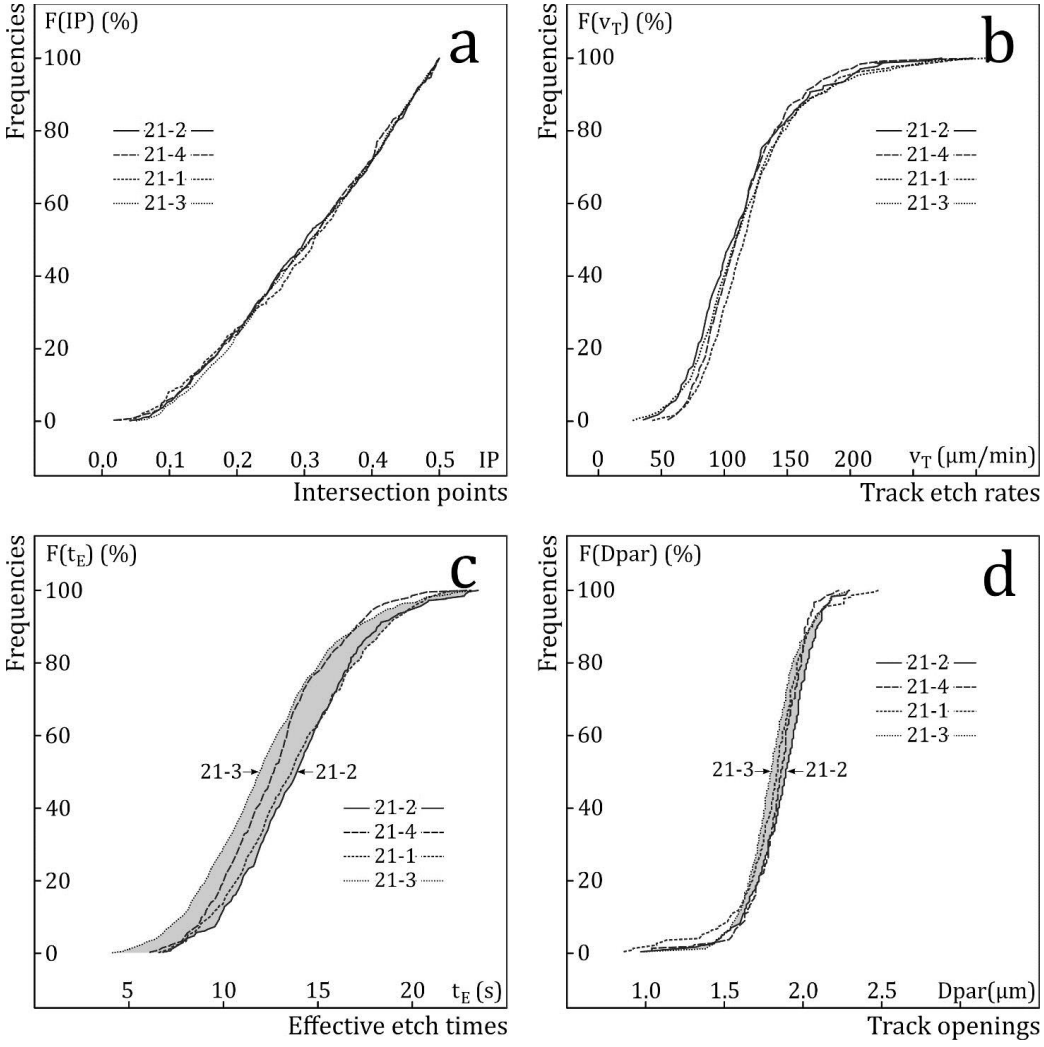

183 **Figure 6. (a)** Cumulative frequencies of the intersections between host-track and confined track, meas-
184 ured from the intersection to the closest track tip and normalised to the confined track length. **(b)** Cu-
185 mulative frequencies of the calculated track etch rates v_T. **(c)** Cumulative frequencies of the calculated
186 effective etch times t_E **(d)** cumulative frequencies of the size of the track surface intersections parallel
187 to the ***c***-axis (Dpar).

https://doi.org/10.5194/egusphere-2026-889
Preprint. Discussion started: 16 March 2026

LSTD	N_C	$l_M(\sigma)$	s_M	l_{50}	$l_P(\sigma)$	s_P	l_{P50}	$l_C(\sigma)$	$l_A(\sigma)$	$l_{PC}(\sigma)$	$l_{PA}(\sigma)$
21-2	572	15.9(1)	0.75	15.9	16.3(1)	0.56	16.3	16.3(1)	15.7(1)	16.1(1)	16.4(1)
21-4	370	14.2(1)	0.77	14.3	15.1(1)	0.52	15.1	15.1(1)	13.8(1)	14.9(1)	15.2(1)
21-1	332	11.9(1)	0.90	11.8	13.5(1)	0.46	13.5	13.5(1)	11.1(1)	13.3(1)	13.6(1)
21-3	801	10.1(1)	1.49	10.3	12.5(1)	0.47	12.5	12.4(1)	9.3(1)	12.2(1)	12.7(1)

LSTD	N_E	$t_{EM}(\sigma)$	s_{TE}	t_{E50}	N_{VT}	$v_{TM}(\sigma)$	s_{VT}	v_{T50}	N_D	Dpar(σ)	s_D	D_{50}
21-2	568	13.3(1)	3.4	12.4	607	127(2)	44	114	219	1.81(2)	0.25	1.89
21-4	368	12.2(2)	3.0	11.4	426	123(2)	41	111	231	1.87(2)	0.20	1.86
21-1	329	13.2(2)	3.2	12.4	328	123(3)	47	107	239	1.80(1)	0.19	1.84
21-3	799	11.5(1)	3.5	10.4	697	123(2)	48	105	212	1.84(1)	0.18	1.80

Table 2. Measurements of confined tracks in unannealed and part-annealed prism faces of Durango apatite etched for 20s in 5.5 M HNO_3 at 21 °C. N_C: number of confined track lengths; l_M: mean length (µm); s_M: standard deviation (µm); l_{50}: median; l_P: mean ***c***-axis-projected length (µm); s_P: standard deviation of the projected lengths (µm); l_{P50}: median projected length;(l_C, l_A): ***c***-axis and ***a***-axis intercepts of ellipses fitted to length vs. orientation data (µm); (l_{PC}, l_{PA}): ***c***-axis and ***a***-axis intercepts of regression lines to projected length vs. orientation data (µm). N_D: Number of Dpar-measurements; Dpar: mean Dpar (µm); s_D: standard deviation (µm); D_{50}: median (µm); N_E: number of effective-etch-time measurements; t_{EM}: mean effective etch time (s); s_{TE}: standard deviation (s); t_{E50}: median effective etch time (s); N_{VT}: number of track etch rate measurements; v_{TM}: mean track etch rate (µm.min^{-1}); s_{VT}: standard deviation (µm.min^{-1}); v_{T50}: median track etch rate (µm.min^{-1}). Numbers in brackets are standard errors of the corresponding statistic.

The median effective etch time of the unannealed tracks (21-2) is 2 s longer than that of the most annealed (21-3; Figure 6c). Both intermediate samples lie between the extremes, albeit in reverse order. Given that their track and apatite etch rates are almost the same, one could expect that t_E correlates with the reciprocal track densities. That of 21-3 is ~⅔ of 21-2 (Aslanian et al., 2022); the average separation between a host track and a potential confined track in 21-3 is thus greater than in 21-2. However, this must not be the case for the measured tracks, selected on the basis of their widths. For an average v_T of ~2 µm.s^{-1} (Table 2: ~120µm.min^{-1}), a ~2-s t_E-difference corresponds to a ~4-µm difference of the etchant trajectories from the host track intersections to the confined track tips. This is in broad agreement with the ~6 µm mean length difference between 21-2 and 21-3.

All samples have narrow Dpar-distributions with medians (D_{50}) decreasing from 1.89 µm for the unannealed apatite (21-2) to 1.80 µm for the most annealed (21-3). The difference is small but reflects a systematic shift of the Dpar-distribution to lower values with increasing annealing (Figure 5d). Because Dpar is proportional to the apatite etch rate, it suggests a thermal relaxation of irradiation-induced strain from recoils following (n,γ)-reactions or uranium fission and track formation (Rivera et al., 2011; Dufour and Toulemonde, 2016; Schauries, 2018; Rymzhanov et al., 2019). Assuming Arrhenius kinetics, the D_{50}-ratio (1.80/1.89 = 0.953) for the most annealed and unannealed samples represents an increase of the activation energy for apatite etching of 118 J.mol^{-1}, or 1.22 meV per atom. If an individual point defect stores ~1 eV, the lowering of the apatite etch-rate results from annealing one in a thousand (F_D = 1.22 10^{-3}) defects created by irradiation.

For Arrhenius kinetics, the rate factor (k_D) and activation energy (E_D) for defect annealing are given by:

$$k_D = \frac{ln(1-F_D)}{t_A} = 3.3910^{-8}s^{-1} \quad (1)$$

https://doi.org/10.5194/egusphere-2026-889
Preprint. Discussion started: 16 March 2026

wherein t_A = 36000 s is the annealing time (10 h). For a pre-exponential factor $k_0 = 10^{13}$ s^{-1}, this gives:

$$E_D = RT_A ln\left(\frac{k_0}{k_D}\right) = 228 \text{ kJ. mol}^{-1} \quad (2)$$

wherein R = 8.314 $J.K^{-1}.mol^{-1}$ is the gas constant and T_A = 310 °C the annealing temperature of sample 21-3. For comparison, we calculated similar rate factors (k_F) and activation energies (E_F) for fission-track annealing using the fractional length reduction, $F_F = 1 - l/l_0$, as the measure of progress. This shows that E_F increases from 182 kJ mol^{-1} at 240 °C to 200 kJ mol^{-1} at 310 °C (Table 3). Without attaching undue meaning to the specific numbers, it bears out that fission-track annealing and the partial elimination of point defects that causes a decrease of the apatite etch rate are processes that occur in parallel under the annealing conditions to which the samples were subjected. Point defects begin to anneal at Tt-conditions at which fission-track annealing is well advanced.

LSTD	T_A (°C)	t_A (h)	T_A (K)	t_A (s)	F_F	k_F ($10^{-6}.s^{-1}$)	E_F ($kJ.mol^{-1}$)
21-4	240	10	513	36000	0.11	3.14	182
21-1	288	10	561	36000	0.25	8.05	194
21-3	310	10	583	36000	0.36	12.6	200

Table 3. Activation energies for fission-track annealing. T_A: annealing temperature in °C and in K; t_A: annealing time in hours and in seconds; F_F: fractional annealing $F_F = 1 - l/l_0$; k_F: rate factor; E_F: activation energy.

For a constant-core model and high average track etch rate ($v_T \approx 120$ µm.min^{-1}; Table 2), the exact value of v_T and the precise point from where a confined track begins to etch are of little consequence. For the same reason, the effect of multiple host track intersections, even occurring at the same time and far apart, is minimal. This is not so for a linear v_T-profile with a central maximum (~1.7 µm.s^{-1}; unannealed induced tracks) decreasing to v_R towards the track tips (Ketcham and Tamer, 2021). In that case, short tracks intersected towards one end have a higher likelihood than longer tracks to be etched at the opposite end to a point that satisfies an operator's selection criteria. This would result in a positive correlation between the track length and the position of the host track intersection (Figure 8 of Jonckheere, 2023). The correlation would decrease depending on the extent of length reduction and the increased track etch rate after partial annealing (Ketcham and Tamer, 2021).

Supplement Figures S07 - S09 show the dependence of the ***c***-axis-projected lengths (l_P) of individual tracks in each sample on IP, v_T, and t_E. Two regression lines to l_P vs. IP have small positive and two have small negative slopes (Table 4), suggesting the absence of significant correlation. The regression lines to l_P vs. v_T have small positive slopes. Because of the large v_T-range (Supplement Figure S5), this nonetheless adds ~0.1 - 0.3 µm to the lengths of fast-etching compared to slow-etching tracks. We reported positive correlations between l_P and t_E of fossil (Aslanian et al., 2021) and induced tracks (Jonckheere et al., 2024a) in Durango apatite, based on repeat measurements of individual step-etched tracks. In contrast, Supplement Figure S9 compares l_P and t_E measurements of different tracks in a population etched once. The fact that the plots indicate far less correlation (none in 21-4) is in part due to the limited t_E-range (Supplement Figure S6) and statistical factors. The correlation adds ~0.1 - 0.3 µm to the lengths of well-etched ($t_E \approx 20$ s) compared to underetched ($t_E \approx 5$ s) tracks. We nevertheless conclude that, for practical purposes, neither the intersection point, the track etch rate or the effective etch time have a significant effect on length measurements of confined tracks etched once (20 s; 5.5 M HNO_3; 21 °C). This does however not mean that these factors also have negligible effect on the selection of confined tracks for measurement.

https://doi.org/10.5194/egusphere-2026-889
Preprint. Discussion started: 16 March 2026

LSTD	I(v_T)	S(v_T)	Δ(v_T)	Δ%	I(t_E)	S(t_E)	Δ(t_E)	Δ%
21-2	16.25	0.001	0.13	0.8	16.21	0.007	0.11	0.7
21-4	14.93	0.001	0.23	1.5	15.11	-0.001	-0.01	-0.1
21-1	13.38	0.001	0.22	1.6	13.24	0.017	0.28	2.1
21-3	12.36	0.001	0.30	2.4	12.41	0.006	0.11	0.9
DULU	I(v_T)	S(v_T)	Δ(v_T)	Δ%	I(t_E)	S(t_E)	Δ(t_E)	Δ%
FC1-I	16.22	0.0004	0.10	0.6	15.95	0.030	0.58	3.6
FC1-S	13.48	0.0031	0.67	4.9	13.90	0.007	0.14	1.1
AS3-I	16.22	0.0006	0.15	0.9	15.83	0.034	0.66	4.2
AS3-S	13.94	0.0008	0.17	1.2	13.69	0.027	0.57	4.5

Table 4. Relationship between ***c***-axis-projected lengths (l_P), track etch rates (v_T), and effective etch times (t_E). I(...)and S(...): intercepts and slopes of regression lines fitted to l_P versus v_T and l_P versus t_E; Δ(.): maximum difference over the range of v_T- and t_E- values; Δ%: percent difference.

4. Effect of ageing

We analysed the FC1 and AS3 apatites from the Duluth intrusive complex in Minnesota to investigate the effects of geological ageing. These well-studied samples are reference materials and proposed age standards (Iwano et al., 2019; Härtel et al., 2022; 2023). Their interest lies in the fact that they are old and have long low-temperature thermal histories, permitting the accumulation of extensive radiation damage, the most important factor with respect to ageing. Based on data of Härtel et al. (2023), the total alpha dose for FC1 is ~7.10^{16} a.g^{-1} (0.8-1.0 dpa), although it is not known which fraction of the accumulated damage survived till the present. We annealed an aliquot of FC1 and AS3 for 24 h at 450 °C, and irradiated it with thermal neutrons in channel Y4 of the BR1 reactor in Mol, Belgium. We mounted an irradiated and an untreated fraction of each in resin, and ground, polished and etched them using the techniques described in section 3. As there also, we measured the track lengths, orientations, widths, cone-angles, and Dpar, but not the host track intersections, and calculated the effective etch times and the apatite and track etch rates.

Consistent with their similar Dpar-values, the induced-track length distributions of FC1 and AS3 are almost identical. The fossil tracks in both samples underwent >20% shortening; both fossil-track length distributions are also similar, albeit that those in FC1 are somewhat shorter. We interpret this difference as significant; ***c***-axis projection highlights the greater fraction of short tracks (Table 5; Figure 7a,b). The semi-axes of ellipses fitted to the induced-track data are close to the trend for unannealed apatites (Donelick et al., 1999); those fitted to the fossil-track data reveal them to be somewhat less anisotropic than induced tracks of the same mean length (Figure 7c). This could be due to different length bias affecting high- and low-angle tracks, different angular distributions, which control the relative weights of the constituent populations, or under-etching (Jonckheere, 2023; Jonckheere et al., 2024). However, the angular distributions of the fossil, as well as induced, tracks are almost identical (Figure 7d) and the effective etch times of the fossil tracks are 1-2 s longer than those of the induced (Table 3; Figure 8b). This argues against experimental factors. This leaves length-bias or unknown differences between fossil and induced tracks.

https://doi.org/10.5194/egusphere-2026-889
Preprint. Discussion started: 16 March 2026

DULU	N_C	$l_M(\sigma)$	s_M	l_{50}	$l_P(\sigma)$	s_P	l_{P50}	$l_C(\sigma)$	$l_A(\sigma)$	$l_{PC}(\sigma)$	$l_{PA}(\sigma)$
FC1-I	536	15.9(1)	0.83	15.9	16.3(1)	0.60	16.3	16.1(1)	15.8(1)	16.1(1)	16.4(1)
FC1-S	527	12.4(1)	1.49	12.5	13.8(1)	1.00	13.9	13.2(2)	12.0(1)	13.3(1)	14.2(1)
AS3-I	346	15.8(1)	0.86	15.8	16.2(1)	0.63	16.3	16.1(1)	15.6(1)	16.1(1)	16.3(1)
AS3-S	309	12.6(1)	1.36	12.7	14.0(1)	0.88	14.0	13.6(2)	12.1(1)	13.7(1)	14.2(1)

DULU	N_D	Dpar(σ)	s_D	D_{50}	N_E	$t_{EM}(\sigma)$	s_E	t_{E50}	N_{VT}	$v_{TM}(\sigma)$	s_{VT}	v_{T50}
FC1-I	406	2.06(2)	0.34	2.11	460	10.6(2)	3.8	10.6	460	105(2)	42	99
FC1-S	384	2.41(2)	0.30	2.47	513	13.1(2)	4.1	13.1	503	99(2)	39	97
AS3-I	381	1.92(1)	0.26	1.97	300	11.2(2)	3.7	10.9	300	107(2)	41	100
AS3-S	390	2.23(1)	0.28	2.27	268	12.2(3)	4.0	12.0	267	99(3)	42	93

Table 5. Measurements of fossil and induced confined tracks in FC1 and AS3 apatite, etched for 20s in 5.5 M HNO_3 at 21 °C. See Table 1 for symbols.

As in the case of the annealed Durango samples, the track-etch-rate distributions of all the Duluth samples are almost identical (Figure 8a). The ~5% difference between the means for the fossil and the induced tracks (Table 3) is too small to call it significant at this stage. The overall agreement is striking given that the track etch rates v_T are calculated from the apatite etch rates v_R (Fu et al., 2024):

$$v_T = \frac{S_{12}}{(D_1 - D_2)} v_{R,S} \quad (3),$$

wherein S_{12} is the distance between two inscribed circles, with diametres D_1 and D_2, touching facing sides of the confined track, and v_{RS} is the apatite etch rate perpendicular to the track axis. Dpar-measurements indicate that the apatite etch rate differs 7 - 8% between FC1 and AS3 and 16-17% between the fossil and induced tracks (Table 3). We applied the empirical correlation between Dpar and v_R (Fu et al., 2024; Trilsch et al., 2024) for calculating the apatite etch rates of each sample:

$$v_{R,S} = \frac{Dpar_S}{Dpar_D} v_{R,D} \quad (4).$$

$Dpar_S$ and $Dpar_D$ refer to the sample and to Durango apatite, and $v_{R,D}$ is the etch rate of Durango (Aslanian et al., 2021). The agreement between the v_T-distributions of FC1 and AS3 is perhaps unsurprising. Both are from the Duluth complex anorthosite series, albeit from locations >100 km apart, and, according to their ages and track length distributions, both had similar thermal histories. The less obvious fact is that, in contrast to the substantial length reduction, ageing, or low-temperature geological annealing, appears to have a minimal effect on the etch rates of confined tracks.

As in the case of the annealed Durango samples, the average effective etch-times (t_E) of FC1 and AS3 are just over half the immersion time (t_I = 20 s; Table 3). The means, medians and standard deviations for both induced-track samples are similar, those for both fossil-track samples somewhat less so, reflecting different geological histories. There is, on the other hand, a distinct separation between the t_E-distributions of the fossil and induced tracks (Figure 8b,d), which is not due to v_T. The longer effective etch times of the fossil tracks are instead due to the greater v_R of the fossil-track grains, which enable faster etchant access to the confined tracks. There are contributing factors: the much higher fossil than induced track densities (Jonckheere et al., 2024a) lowers the average separation between the host tracks and confined tracks; on the other hand, the shorter fossil- than induced-track lengths have an opposite effect. It is difficult to separate these factors because the stock of confined tracks is filtered through the scientist's selection criteria.

https://doi.org/10.5194/egusphere-2026-889
Preprint. Discussion started: 16 March 2026

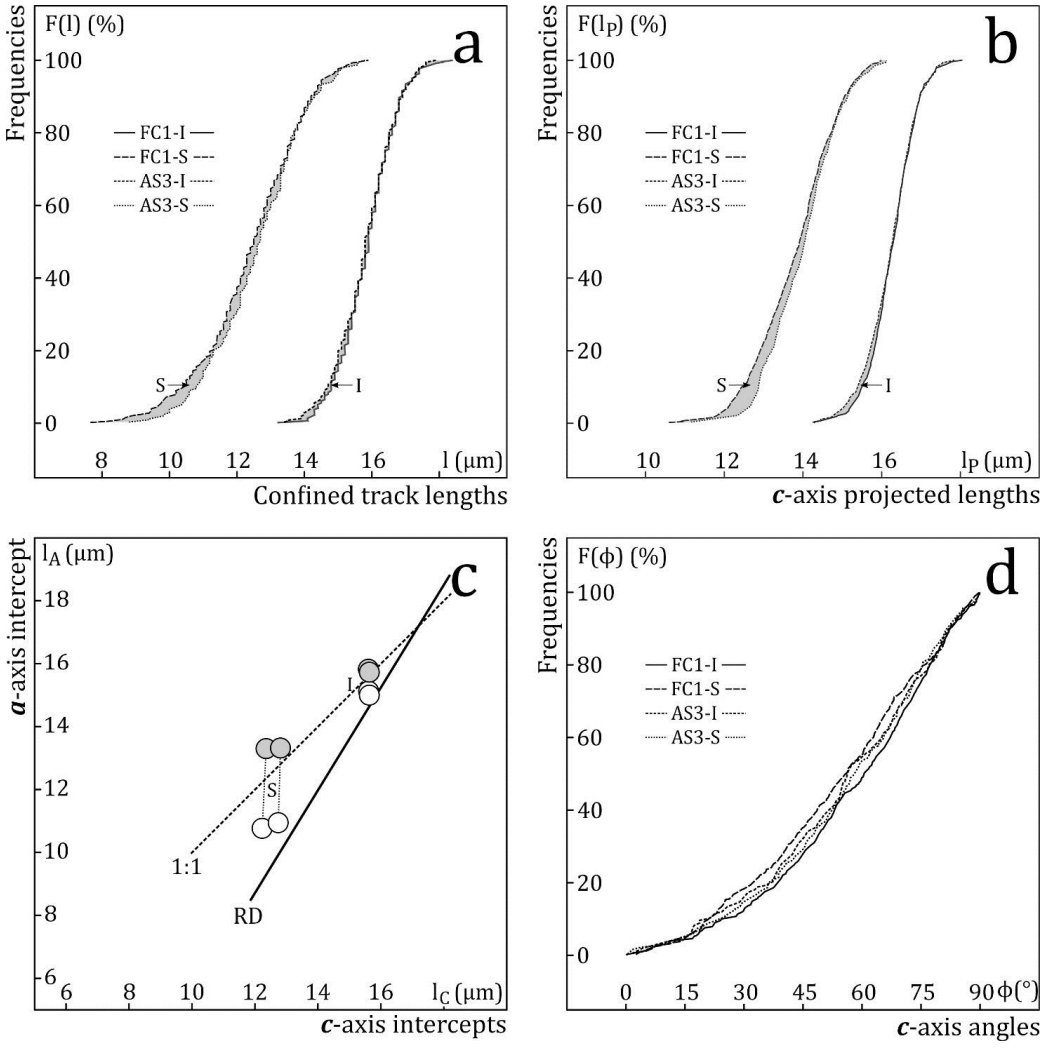

Figure 7. (a) Cumulative frequencies of the lengths of fossil (S) and induced (I) confined tracks in prism faces of FC-1 and AS-3 apatites from the Duluth complex, Minnesota, USA (Iwano et al., 2019; Härtel et al., 2023). **(b)** Cumulative frequencies of the ***c***-axis projected lengths of FC-1 and AS-3. **(c)** ***a***-axis vs. ***c***-axis intercepts of ellipses fitted to the lengths and regression lines fitted to the ***c***-axis projected length vs. ***c***-axis angle (white: induced; grey: fossil; RD and 1:1 as in Figure 5); **(d)** cumulative frequencies of the ***c***-axis angles.

https://doi.org/10.5194/egusphere-2026-889
Preprint. Discussion started: 16 March 2026

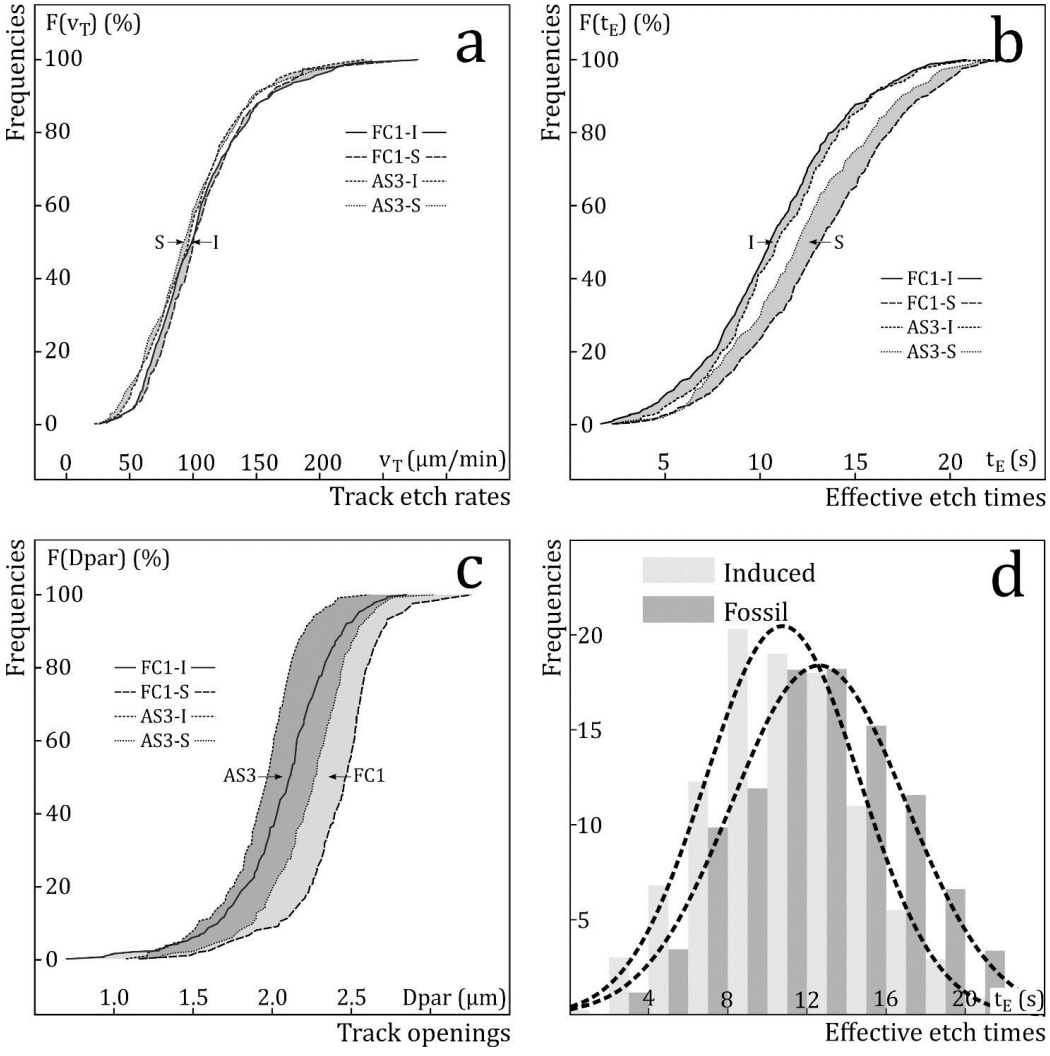

Figure 8. (a) Cumulative frequencies of the track etch rates of fossil (S) and induced (I) confined tracks in the FC-1 and AS-3 apatites **(b)** Cumulative frequencies of the effective etch times of fossil and induced tracks **(c)** cumulative frequencies of the sizes of the track surface intersections (Dpar) of fossil and induced tracks. (d) Histograms of the effective etch times of the combined fossil and induced tracks of FC-1 and AS-3.

https://doi.org/10.5194/egusphere-2026-889
Preprint. Discussion started: 16 March 2026

The clearest distinction between FC1 and AS3, and between fossil and induced tracks, is in their Dpar's (Table 3; Figure 8c). The Dpar's of fossil-tracks are 16%(AS3)-17%(FC1) higher than those of induced tracks. We propose that this is due to distributed radiation damage from α-disintegration of ^{238}U, ^{235}U, ^{232}Th, and ^{146}Sm, and collateral recoils from ^{238}U-fission, accumulated over geological time. The resulting lattice damage increases the overall apatite etch rate, leading to larger Dpar. Figure 9 shows the Dpar's of fossil and induced tracks in FC1. The ageing of the fossil-track samples appears to have a much greater effect on Dper than on Dpar. This supports the radiation damage concept: Dpar depends on the etch rate of fast etching apatite faces while Dper is controlled by the slow-etching prism faces flanking the track on either side (Jonckheere et al., 2022). Slow-etching faces are more susceptible to radiation damage than fast etching faces (Jonckheere et al., 2019), which accounts for the doubling of Dper, while Dpar increases <20% on average (Figure 9b).

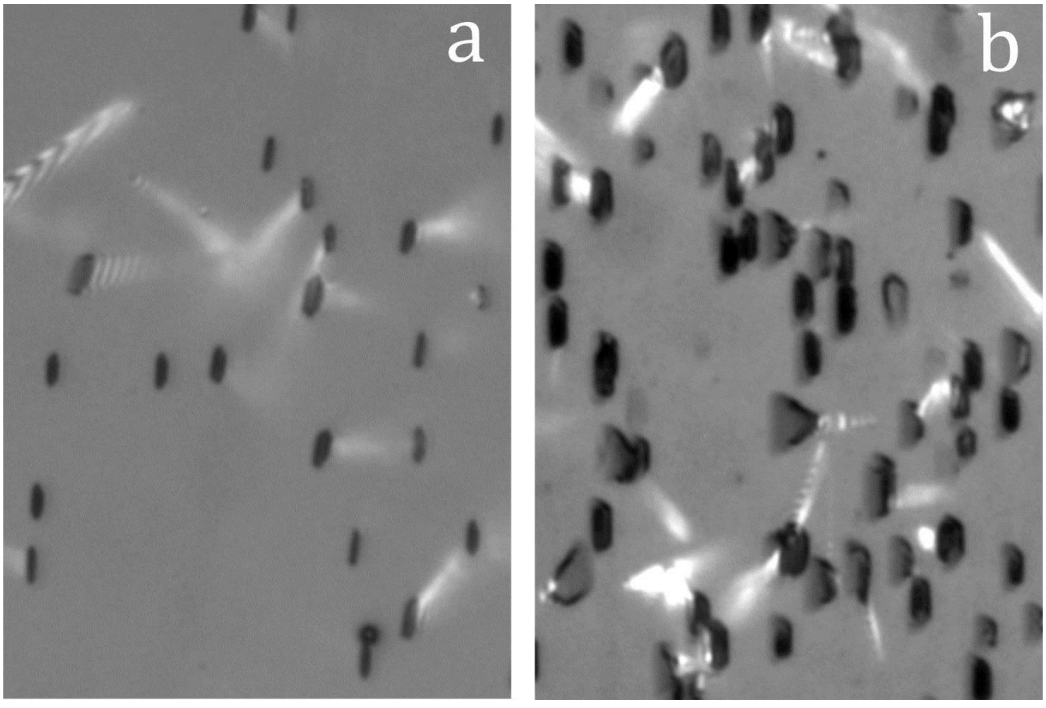

Figure 9. Reflected-light images of the openings of induced **(a)** and fossil **(b)** tracks in prism faces of the FC1 apatite (etched 20 s in 5.5 M HNO_3 at 21 °C).

4. Conclusion

Since the earliest fission track studies, all etch models have been based on two velocities: v_T, the rate of advance along the damaged core, and v_R, the rate of retreat of the undamaged material. These velocities are more than conceptual: their values define the efficiencies of the track counts (Tagami and O'Sullivan, 2005) and set the thresholds for confined-track selection (Ketcham and Tamer, 2021). They form furthermore the basis for explaining the shapes of etched tracks (Jonckheere et al., 2022). On its own, v_R is an important indicator of chemical composition and annealing kinetics (Dpar; Burtner et al., 1994). Despite this, measurements of v_T and v_R have long been lacking. This work aims to fill this gap to some extent and to investigate some factors controlling v_R and v_T.

https://doi.org/10.5194/egusphere-2026-889
Preprint. Discussion started: 16 March 2026

Direct measurements and microscopic observation indicate that v_T is constant over most of the length of ion and fission tracks in apatite (constant core model; Tamer and Ketcham, 2020). This suggests that there is a threshold damage above which v_T does not increase, e.g., an amorphous core raises v_T to a value that does not depend on the work expended to create it (amorphous is amorphous). This is however not a conclusion within the compass of our investigation. On the other hand, reconciling straight-sided etched surface and confined tracks with something other than a constant v_T requires a different and more complex etch model than any proposed to date. Our results revealed that the etchant advances at a high but finite rate along pre-etched tracks. This implies that the summed immersion times of step-etch experiments are overestimates, and that step-etching broadens the effective-etch-time distribution (Figure 6a of Jonckheere et al., 2024a). It also implies that successive etch steps cause v_T to be underestimated to an increasing extent (Figure 5c of Jonckheere et al., 2024a). The low v_T of Aslanian et al. (2021; ~75 µm.min^{-1}) for fossil tracks in Durango apatite must therefore be read as an underestimate, consistent with the present results.

The distributions of host-track intersections (IP), ***c***-axis angles (ϕ), and track-etch rates (v_T) are almost identical across all measurements. There is a notable offset between the average v_T of the Durango and Duluth samples, but this need not mean that it is also of fundamental significance. The calculation of v_T requires v_R, which was measured for Durango (Aslanian et al., 2021) and other apatites (Trilsch et al., 2023; Fu et al., 2024), but not for FC1 and AS3, whose etch rates were estimated from their Dpar's, relative to that of Durango. The v_T-difference between Durango and Duluth could be within the scope of this approximation, which could also account for the small difference between the fossil and induced tracks in FC1 and AS3. The near-identical IP-, ϕ-, and v_T-distributions are difficult to explain, but suggest that the confined-track selection is dominated by a criterion that is more or less independent of the track densities or lengths. The confined-track width is such a criterion that is moreover little affected by annealing (Jonckheere, 2023).

In contrast to the track etch rate v_T, the apatite etch rate v_R shows marked variation. This is most obvious from the Dpar's of the fossil and induced tracks in FC1 and AS3, but also from those of the part-annealed induced tracks in Durango. In the case of the fossil tracks, the Dper/Dpar-ratio increases as well as, and faster than Dpar. It is therefore probable that the increases are related to radiation damage, from the natural background radiation in the fossil-track samples and neutron irradiation in the induced-track samples. Dper/Dpar offers a means of assessing damage densities in apatite if we can separate their effect from the chemical control of Dpar. On the other hand, this Dpar-variation reveals the need for caution when using Dpar for estimating apatite annealing kinetics. The increased v_R of the Duluth samples with fossil tracks increases the rate of advance of the etchant along the slowest section of its course down the host track (v_T), across to the confined track (v_R; widening of the host track) and along its length to each tip (v_T). Confined tracks in apatites with higher v_R therefore have shorter access times and, in consequence, longer effective etch times.

5. Acknowledgment

We thank the accelerator staff at the Heavy Ion Research Facility Lanzhou of the Institute of Modern Physics of the Chinese Academy of Sciences for their expert handling of the Kr-irradiation.

6. Funding

Funded by the German Science Foundation (Grant JO 358/6).

https://doi.org/10.5194/egusphere-2026-889
Preprint. Discussion started: 16 March 2026

7. References

Aslanian C., Jonckheere R., Wauschkuhn B., Ratschbacher L. (2021) A quantitative description of fission-track etching in apatite. American Mineralogist 106, 518-526.

Aslanian C., Jonckheere R., Wauschkuhn B., Ratschbacher L. (2022) Short communication: Experimental factors affecting fission-track counts in apatite. Geochronology 4, 109-119.

Burtner R.L., Nigrini A., Donelick R.A. (1994) Thermochronology of Lower Cretaceous source rocks in the Idaho-Wyoming thrust belt. American Association of Petroleum Geologist Bulletin 78, 1613-1636.

Carlson W.D., Donelick R.A, Ketcham R.A. (1999) Variability of apatite fission-track annealing kinetics: I. Experimental results. American Mineralogist 84, 1213-1223.

Donelick R.A. (1991) Crystallographic orientation dependence of mean etchable fission track length in apatite: An empirical model and experimental observations. American Mineralogist 76, 83-91.

Donelick R.A., Ketcham R.A., Carlson W.D. (1999) Variability of apatite fission-track annealing kinetics: II. Crystallographic orientation effects. American Mineralogist 84, 1224-1234.

Dufour C., Toulemonde M. (2016). Models for the Description of Track Formation. In: W. Wesch and E. Wendler, eds., Ion Beam Modification of Solids, Springer Series in Surface Sciences, 61, 63-101.

Durrani S.A., Bull R.K. (1987) Solid state nuclear track detection. Principles, methods and applications. Pergamon Press, Oxford, pp. 304.

Fleischer R.L. & Price P.B. (1964) : Techniques for geological dating of minerals by chemical etching of fission fragment tracks. Geochimica et Cosmochimica Acta 28,1705-1714.

Fleischer R.L., Price P.B., Walker R.M. (1975) Nuclear tracks in solids. Principles and applications. University of California Press, Berkeley, pp. 604.

Fleischer R.L., Price P.B., Woods R.T. (1969) Nuclear-particle-track identification in inorganic solids. Physical Review 188, 563-568.

Fu Hongyang, Trilsch F., Jonckheere R., Ratschbacher L. (2024) Compositional effects on the etching of fossil confined fission tracks in apatite. American Mineralogist 109, 2026-2036.

Galbraith, R.F. (2002). Some remarks on fission-track observational biases and crystallographic orientation effects. American Mineralogist 87, 991-995.

Galbraith R.F., Laslett G.M., Green P.F., Duddy I.R. (1990) Apatite fission track analysis: geological thermal history analysis based on a three-dimensional random process of linear radiation damage. Philosophical Transactions of the Royal Society of London A332, 419-438.

Gleadow A.J.W. (1981) Fission track dating methods: what are the real alternatives ? Nuclear Tracks 5, 3-14.

Gross, R. (1918) On the theory of growth and dissolution processes of crystalline matter. Abhandlungen der mathematisch-physischen Klasse der königlichen Sächsischen Gesellschaft der Wissenschaften zu Leipzig 35, 137-202 (in German).

Härtel B., Jonckheere R., Krause J., Ratschbacher L. (2022) Spurious age-eU associations in thermochronology. Earth and Planetary Science Letters, 117870.

Härtel B., Matthews W.A., Enkelmann E. (2023) Duluth complex FC1 apatite and zircon: Reference materials for (U-Th)/He dating? Geostandards and Geoanalytical Research. doi: 10.1111/ggr.12492

Heimann R.B. (1975) Dissolution of crystals. Theory and practical application. Applied Mineralogy 8, Springer, pp. 270 (in German).

Heimann R.B. (1982) Principles of Chemical Etching - The art and science of etching crystals. Silicon Chemical Etching, 173–224. Springer Berlin, Heidelberg.

Hurford A.J., 2019. An historical perspective on fission-track thermochronology. In: M.G. Malusà and P.G. Fitzgerald, Eds., Fission-Track Thermochronology and its Application to Geology, Geography and Environment, 3-23.

Iwano H., Danhara T., Yuguchi T., Hirata T., Ogasawara M. (2019) Duluth Complex apatites: Age reference material for LAICP-MS-based fission-track dating. Terra Nova, 31, 247-256.

Jonckheere R. (2023) On etching, selection and measurement of confined fission tracks in apatite. Geochronology Discussions [preprint].

https://doi.org/10.5194/egusphere-2026-889
Preprint. Discussion started: 16 March 2026

Jonckheere R., Aslanian C., Fu Hongyang, Trilsch F. (2024a) Sampling confined fission tracks for constraining geological thermal histories. Minerals 14, 1-16.

Jonckheere R., Aslanian C., Wauschkuhn B., Ratschbacher L. (2022) Fission-track etching in apatite: A model and some implications. American Mineralogist 107, 1190-1200.

Jonckheere R., Aslanian C., Wauschkuhn B., Ratschbacher L. (2020) Some geometrical properties of fission-track-surface intersections in apatite. American Mineralogist 105, 1355-1364.

Jonckheere R., Härtel B., Iwano H. (2024b) Fission-track age calibration: Phi and Zeta, never the twain shall meet? Chemical Geology 648, 121898.

Jonckheere R., Wauschkuhn B., Ratschbacher L. (2019) On growth and form of etched fission tracks in apatite: A kinetic approach. American Mineralogist 104, 569-579.

Ketcham R.A. (2003) Observations on the relationship between crystallographic orientation and biasing in apatite fission-track measurements. American Mineralogist 88, 817-829.

Ketcham R.A., Carter A., Hurford A.J. (2015) Inter-laboratory comparison of fission track confined length and etch figure measurements in apatite. American Mineralogist 100, 1452-1468.

Ketcham R.A., Donelick R.A., Carlson W.D. (1999) Variability of apatite fission-track annealing kinetics: III. Extrapolation to geological time scales. American Mineralogist 84, 1235-1255.

Ketcham R.A., Tamer M.T. (2021) Confined fission-track revelation in apatite: how it works and why it matters. Geochronology 3, 433-464.

Laslett G.M., Gleadow A.J.W., Duddy I.R. (1984) The relationship between fission track length and track density in apatite. Nuclear Tracks 9, 29-38.

Li Weixing, Kluth P., Schauries D., Rodriguez M.D., Lang M., Zhang Fuxiang, Zdorovets M., Trautmann C., Ewing R.C. (2014) Effect of orientation on ion track formation in apatite and zircon. American Mineralogist 99, 1127-1132.

Li Weixing, Lang M., Gleadow A.J.W., Zdorovets M.V., Ewing R.C. (2012) Thermal annealing of unetched fission tracks in apatite. Earth and Planetary Science Letters 321-322, 121-127.

Li Weixing, Shen Yahui, Zhoua Yueqing, Zhai Pengfei, Nana Shuai, Liu Jie, Ewing R.C. (2023) Unexpectedly narrower track diameter at site of fission event. Earth and Planetary Science Letters 616, 118217.

Nikezić D. (2000) Three-dimensional analytical determination of the track parameters. Radiation Measurements 32, 277-282.

Nikezić D., Yu K.N.(2003) Three-dimensional analytical determination of the track parameters: over-etched tracks. Radiation Measurements 37, 39-45.

Nikezić D., Yu K.N.(2004) Formation and growth of tracks in nuclear track materials. Materials Science and Engineering 46, 51-123.

Paretzke H.G., Benton E.V., Henke R.P. (1973) On particle track evolution in dielectric track detectors and charge identification through track radius measurement. Nuclear Instruments and Methods 108, 73-80.

Rivera A., Garcia G., Olivares J., Crespillo M.L. and Agulló-López F. (2011) Elastic (stress–strain) halo associated with ion-induced nano-tracks in lithium niobate: role of crystal anisotropy. Journal of Physics D: Applied Physics 44, 475301 (11pp).

Rymzhanov R.A., Gorbunov S.A., Medvedev N., Volkov A.E. (2019) Damage along swift heavy ion trajectory. Nuclear Instruments and Methods in Physics Research B 440, 25-35.

Schauries D. (2018) Ion tracks in apatite and quartz and their behaviour with temperature and pressure. Ph.D. Thesis, Australian National University. Springer Theses ISSN 2190-5053,pp. 166.

Somogyi G., Szalay S.A. (1974) Track diameter kinetics in dielectric track detectors. Nuclear Instruments and Methods 109, 211-232.

Tagami T., O'Sullivan P.B. (2005) Fundamentals of fission-track thermochronology. Reviews in Mineralogy and Geochemistry 58, 19-47.

Tamer M.T., Ketcham R.A. (2020) The along-track etching structure of fission tracks in apatite: Observations and implications. Chemical Geology 553, 119809.

Trilsch F., Fu Hongyang, Jonckheere R., Ratschbacher L. (2023) Effective etch times of fossil fission tracks in geological apatite samples and impact on temperature-time modelling. Lithosphere (Special 14), lithosphere_2023_339.